Predicting Cohesive Failure in Thermosets

Douglas B. Adolf,[1] Robert S. Chambers,[2] Brenton Elisberg,[2] Mark Stavig,[1] Mary Ruff[3]

[1]*Sandia National Laboratories, Materials Sciences and Engineering Center, Albuquerque, New Mexico 87185-0958*
[2]*Sandia National Laboratories, Engineering Sciences Center, Albuquerque, New Mexico 87185-0346*
[3]*Department of Materials and Metallurgical Engineering, New Mexico Institute of Mining and Technology, Socorro, New Mexico 87801*

Received 1 March 2010; accepted 6 June 2010
DOI 10.1002/app.32938
Published online 26 August 2010 in Wiley Online Library (wileyonlinelibrary.com).

ABSTRACT: Modeling of stresses in epoxies used as adhesives, coatings, or encapsulants in electronic packaging can guide an engineer to more robust designs and material selections. However, stresses by themselves allow evaluation of qualitative trends only. Quantitative assessment of design margins requires some knowledge of when stresses become excessive and failure is imminent. In this study, stresses were predicted accurately in a wide variety of tests, and the state of stress and strain was examined at the point of experimental failure to extract a single scalar metric that design engineers could use to correlate with the observed initiation of cracking. A value of the maximum principal strain of roughly 40% satisfactorily matched data encompassing different geometries, modes of deformation, and test temperature and is apparently linked to a physical mechanism of failure arising from "run-away" nonlinear viscoelasticity. © 2010 Wiley Periodicals, Inc. J Appl Polym Sci 119: 2143–2152, 2011

Key words: thermosets; failure; modeling

INTRODUCTION

The aim of this article focuses on defining a computational path allowing engineers to make quantitative predictions of the initiation of cohesive failure in thermosets for arbitrary applied deformations, temperatures, and rates. An example of a problem addressed by this approach would include an encapsulated electronic component, where an epoxy has been cured in a mold containing printed wiring boards, cooled to room temperature, removed from the mold, and thermal cycled. No pre-existing crack is observed; however, numerous stress risers of various geometries are present that could act as failure initiation sites during the thermal cycles. It is possible to imagine that a fairly representative finite element mesh could be constructed of this component including the stress risers, since corner radii of curvature in crack-prone components are typically prescribed. Given an accurate constitutive equation for the polymer thermomechanical response, one could calculate stresses and strains in the component. Failure predictions would then require a scalar metric constructed from these computed tensors that portends crack initiation and whose critical value is determined from a well-defined experimental test. A successful metric would predict failure initiation consistently in all situations using this one number implying that validation requires fabrication of families of failure samples with stress risers of varying severity.

The proposed metric is intended for application to failure initiation and not to crack propagation. While initiation of cohesive failure is inherently quasistatic, crack propagation in polymers could involve inertial and thermal complexities. In addition, the local geometry of stress risers such as a "notch" or embedded corner are quite regular when compared to a crack, which can be extremely complex with microcracks, microvoids, and/or multiple tips. This article will focus on developing a criterion for predicting initiation of cohesive failure at these more geometrically regular stress risers and will avoid propagation of a natural crack. Solution of crack propagation has been typically addressed with fracture mechanics, in which such complexities are purposefully ignored.

Very few literature studies have focused on computational predictions of failure initiation in polymers. Predictions of propagation of existing cracks through analytical fracture mechanics or computational cohesive zone elements are much more common.[1] A recent study by Gearing and Anand[2] did propose a polymeric failure metric applicable for well-defined stress risers and compared experimental data to computational simulations (see references within). Three features of the current experimental and computational approach distinguish it from this previous study: (1) a much broader range of

Correspondence to: D. B. Adolf (dbadolf@sandia.gov).

© 2010 Wiley Periodicals, Inc.

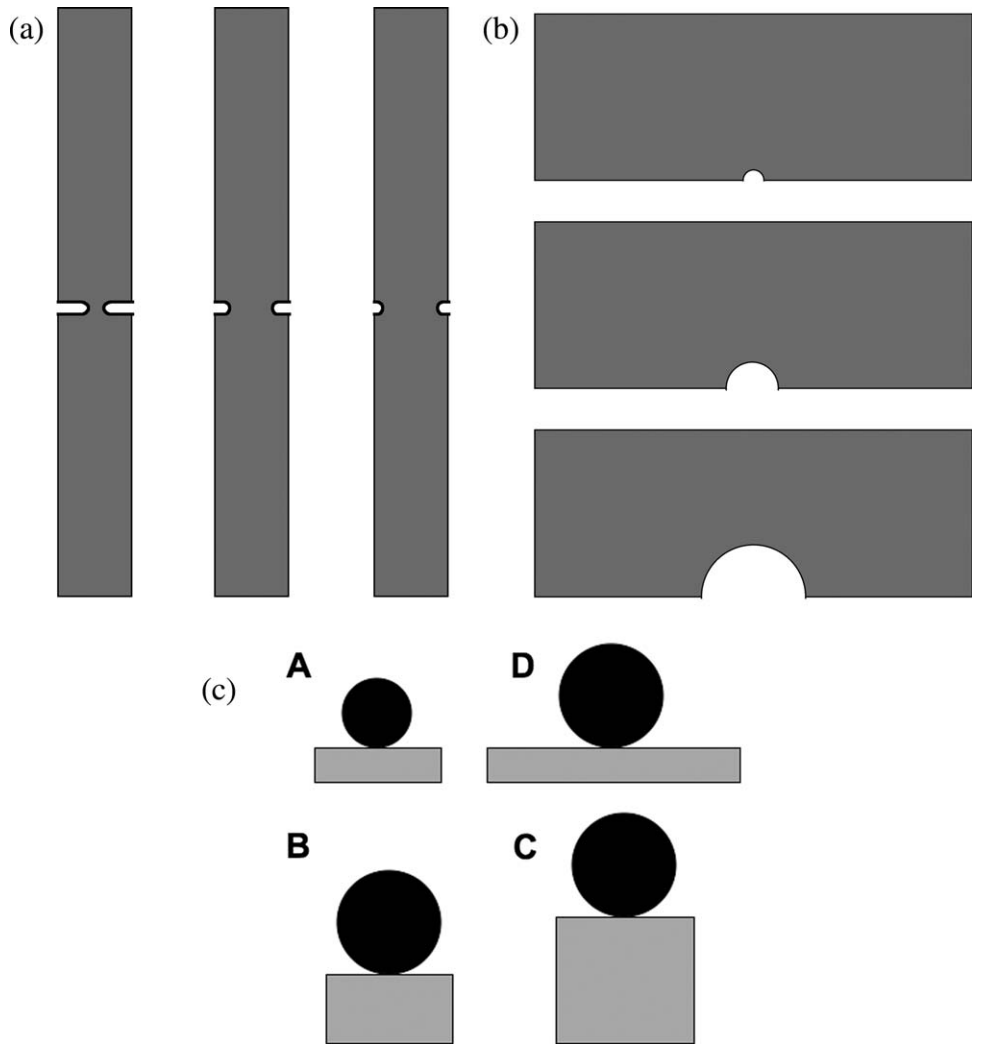

Figure 1 Representative sketches of the sample geometries tested at 22°C to extract a cohesive failure metric. (a) Double notched dog bone. (b) Cylindrically notched three point bend. (c) Ball into a plate.

geometries are examined, (2) test temperatures extending well above and below room temperature are also examined, and (3) an accurate, physically-based, and extensively validated constitutive equation is used to describe the epoxy nonlinear viscoelastic response. A comparison of the conclusions of the current and previous study will be presented after discussion of the data and analyses.

EXPERIMENTAL PROCEDURE

The experimental epoxy presented in Figure 1 consists of the diglycidyl ether of bisphenol A (DGEBA, Epon 828) cured with diethanolamine (DEA, Fisher Scientific) at a ratio of 100-to-12 parts-by-weight. Samples were mixed, degassed, and cured at 70°C for 28 hours resulting in a relatively low glass transition temperature of 70°C. The cure mechanism of this system is quite complex and slow. At 70°C, the secondary amine of DEA completely reacts in 15 minutes to endcap roughly half of the DGEBA. Since the gel time occurs in about 5 hours, it is clear that the crosslinking mechanism involves species other than the secondary amines. At temperatures less than 70°C, this crosslinking mechanism occurs primarily by the tertiary amine-catalyzed condensation of the epoxy with primary or secondary alcohols, while at temperatures above 100°C, the tertiary amine-catalyzed epoxy homopolymerization becomes increasingly important. At intermediate temperatures, both reactions occur. Nevertheless, the change in all thermophysical properties with cure can be reasonably correlated with the empirical extent of reaction defined as the fraction of epoxies reacted. A full characterization of this system has been detailed previously.[3]

Several families of failure samples were fabricated to ensure that the extracted failure metric was generally applicable across a wide range of geometries

TABLE I
Details of the Compressive Failure Tests

Sample designator	Disk diameter (mm)	Disk thickness (mm)	Ball diameter (mm)
A	26	5	13
B	26	12	19
C	26	23	19
D	45	5	19

when tested at the same temperature of 22°C. The first family consisted of simple double notched tensile dog bones with a 100 mm gauge length and cross-sectional dimensions of 12.7 mm × 6.35 mm. At the midpoint of the gauge length, notches of 1, 2, and 3 mm in length were introduced on both sides of the sample with a Buehler cut-off saw and a 0.3 mm thick diamond-coated blade (thus producing a cylindrical notch tip with radius 0.15 mm). Un-notched dog bones were also tested in creep to failure at several stresses for two cooling rates of ~ 0.5°C/min "slow" and 200°C/min "fast," produced by either turning the curing oven off or setting the sample on the lab bench after completion of cure. Another family of three-point bend samples having a 50 mm span and 12.7 mm × 6.35 mm cross-section were prepared with cylindrical "notches" of diameters 1, 4, and 8 mm at the midpoint of the bottom face. These half-cylindrical features were fabricated by abutting two samples and drilling a hole centered at the interface. All these geometries produce a hydrostatic tension near the failure initiation site. To introduce a compressive pressure, disks of epoxy were prepared of various diameters and thicknesses, and a steel ball was driven into the sample until failure. The details of these tests are given in Table I. Representative sketches of the samples from each of these families are pictured in Figure 1.

To investigate the failure mechanisms at different temperatures, two sets of notched three point bend samples were prepared. The notches in the first set were made by the 0.3 mm diameter Buehler saw to depths of 12.7 mm (half-way through the sample). The notches in the second set were standard "pre-cracks." Initial notches were introduced with a diamond saw, and a razor blade was used to propagate a crack roughly half-way through the sample.

Before testing each sample, the samples were annealed by heating to 10°C above the glass transition temperature, holding for 15 minutes, and cooling to the test temperature by turning off the oven (rate measured to be ~ 0.5°C/min). This procedure ensured a consistent thermal history that was modeled in the finite element analyses. All tests were performed on an Instron 1125 load frame. The notched dog bones and three point bend samples were ramped at a rate of 2 mm/min, the "ball into a plate" samples were ramped at 1 mm/min, and the stress was ramped to the required level in 30 sec for the creep tests.

COMPUTATIONAL PROCEDURE

Finite element meshes of all experimental tests were prepared to mimic the actual geometries as closely as possible (examples are shown in Fig. 2). For

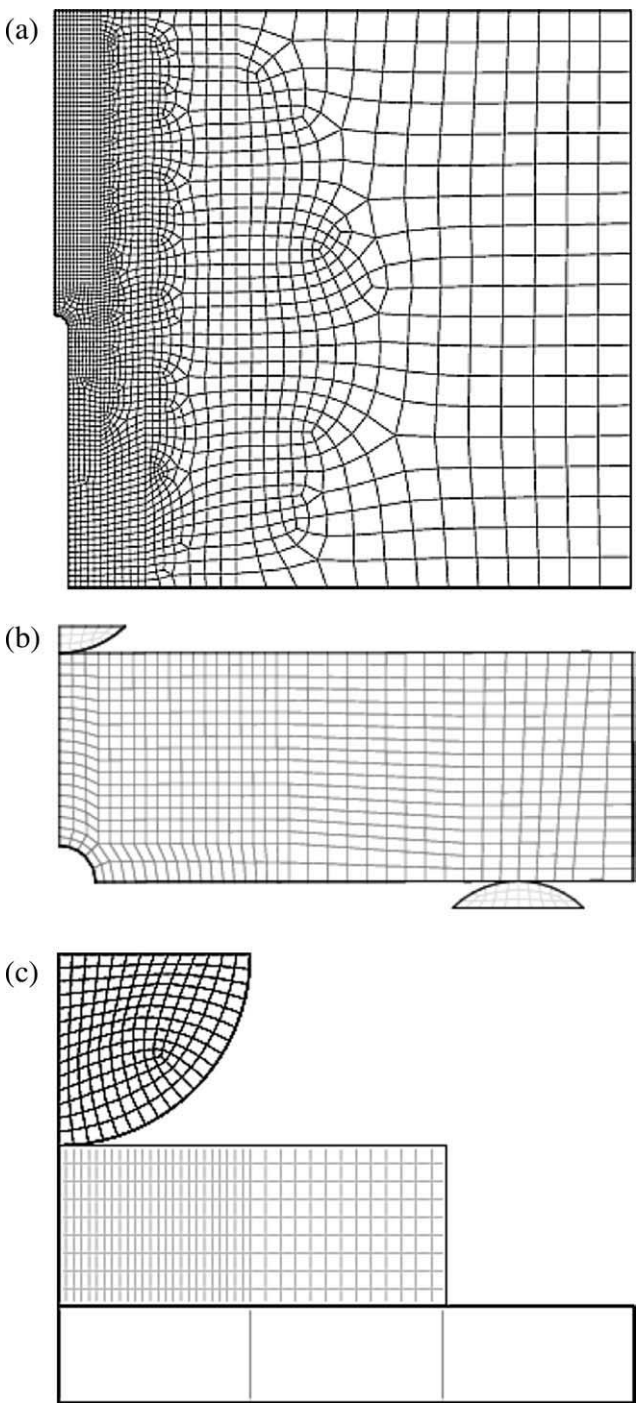

Figure 2 Examples of the finite element meshes used in this study. (a) Double notched dog bone. (b) Cylindrically notched three point bend. (c) Ball into a plate.

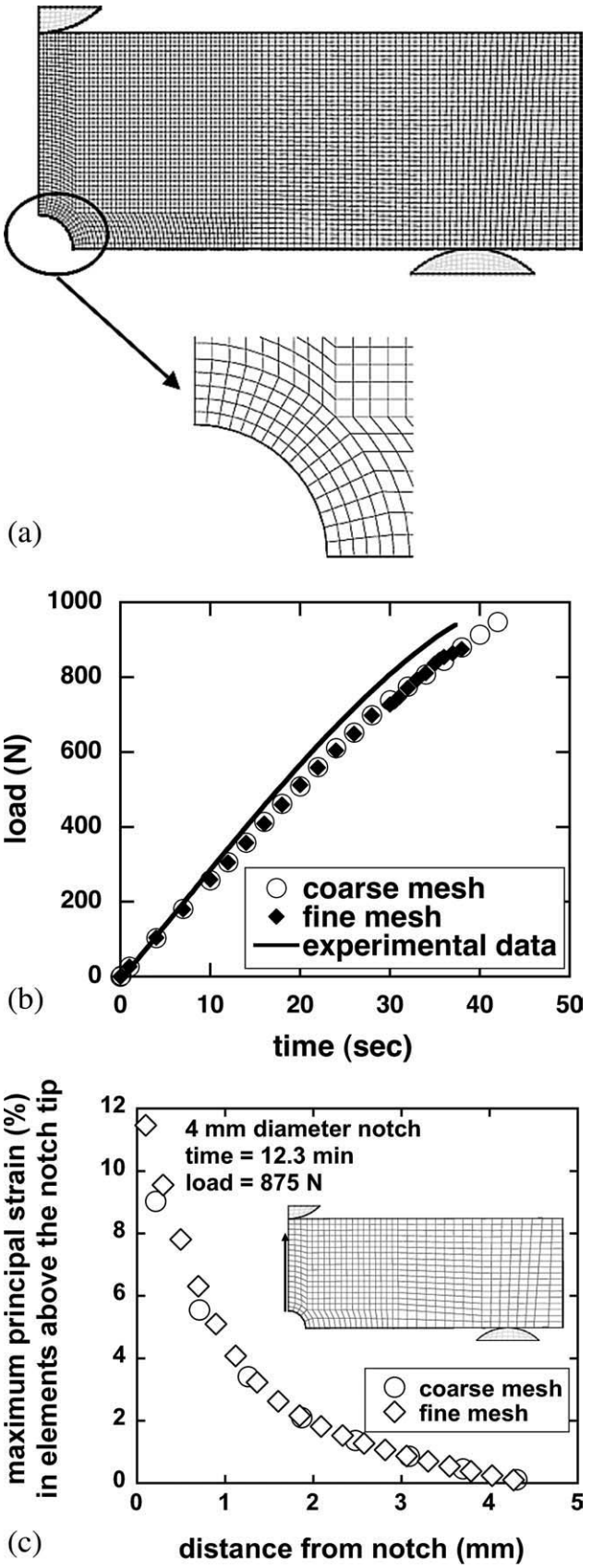

Figure 3 Mesh refinement study for the notched three point bend samples. (a) Fine mesh. (b) Loads predicted from the two meshes. (c) Local strains predicted from the two meshes.

example, the radii of the stress risers and the tests rates were reproduced, the three-point bend supports were modeled, the thermal histories were included, and all analyses were fully three-dimensional. In addition, several studies were undertaken to ensure that the simulation details (mesh refinement, convergence tolerances, friction, etc.) did not introduce systematic error. For example, meshes of the 4 mm diameter notched three point bend samples were created with 10 times more elements [44,136 in Fig. 3(a) vs. 4248 in Fig. 2(b)], and the resultant load-deflection responses were unchanged [Fig. 3(b)]. Even a much more detailed local examination of the maximum principal strains in the elements directly above the notch tip shows no appreciable difference between the two meshes [Fig. 3(c)]. The friction factor in the compressive "ball into a plate" tests was varied from 0 to 0.2, and some sensitivity was observed. The prediction without friction matched the experimental load-displacement response best (Fig. 4).

The epoxy response was modeled with our previously developed, nonlinear viscoelastic constitutive equation employing a potential energy material "clock." The model was derived[4] from a thermodynamically consistent, "Rational Mechanics" approach that uses the Helmholtz free energy as a potential for defining all thermodynamic quantities. Molecular dynamics studies[5] showed that the mobility of simple chain molecules was a unique function of the system's potential energy, and the rational mechanics framework allowed incorporation of this observation into the constitutive equation. To facilitate acceptance and ease of use, the model was subsequently simplified.[6]

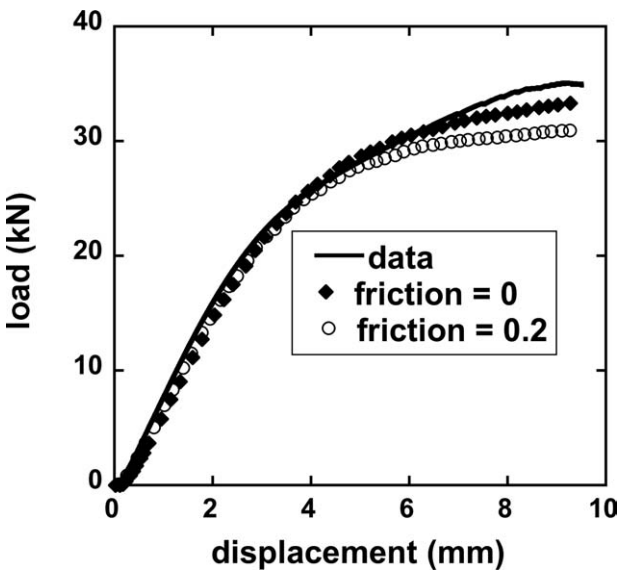

Figure 4 Predicted load-displacement curves for the compressive "ball into a plate" tests using two friction factors and compared to the experimental data.

$$\underline{\underline{\sigma}} = \frac{\rho}{\rho_{ref}}\left[K_d(T)\int_0^t ds\, f_v(t^*-s^*)\frac{dI_1}{ds} - L_d(T)\int_0^t ds\, f_v(t^*-s^*)\frac{dT}{ds}\right]\underline{\underline{I}} + \frac{2\rho G_d(T)}{\rho_{ref}}\int_0^t ds\, f_s(t^*-s^*)\left[\underline{\underline{R}}(t)\cdot\underline{\underline{d}}_{dev}(s)\cdot\underline{\underline{R}}(t)^{-1}\right] + \frac{\rho}{\rho_{ref}}[K_\infty(T)I_1 - L_\infty(T)\{T-T_{ref}\}]\underline{\underline{I}} + \frac{2\rho G_\infty(T)}{\rho_{ref}}\left[\underline{\underline{R}}\cdot\underline{\underline{\varepsilon}}_{dev}\cdot\underline{\underline{R}}^{-1}\right] \quad (1)$$

where $t^*-s^* = \int_s^t \frac{dx}{a(x)}$ and $\log a = -\frac{C_1 N}{C_2'' + N}$

$$N = \left[\{T-T_{ref}\} - \int_0^t ds\, f_v(t^*-s^*)\frac{dT}{ds}\right] + C_3\left[I_1 - \int_0^t ds\, f_v(t^*-s^*)\frac{dI_1}{ds}\right] + C_4\int_0^t\int_0^t ds\, du\, f_s(t^*-s^*, t^*-u^*)\underline{\underline{d}}_{dev}(s) : \underline{\underline{d}}_{dev}(u) \quad (2)$$

σ is the Cauchy stress, d_{dev} is the deviatoric unrotated rate of deformation tensor, ε is its integral, T is temperature, and ρ is density (ρ_{ref} is the density at the arbitrary, unstrained reference state). The required material properties are typical: the decaying and equilibrium bulk and shear moduli (K_d, K_∞, G_d, G_∞), the decaying and equilibrium coefficients of thermal expansion ($L_d = K_d\alpha_d$, $L_\infty = K_\infty\alpha_\infty$), and

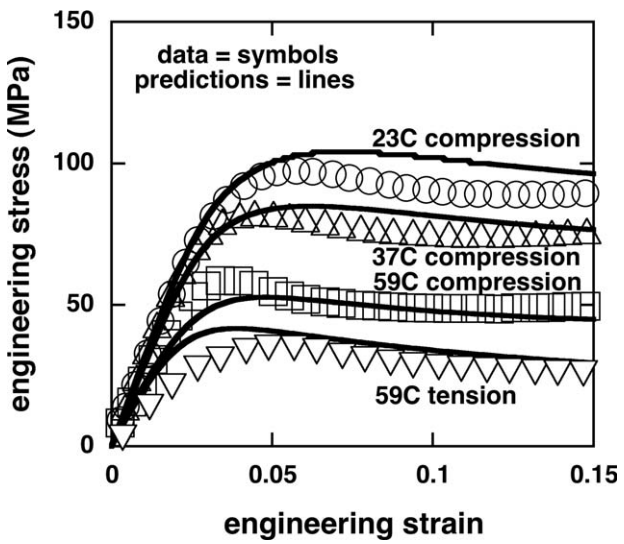

Figure 5 Yield of the DEA-cured epoxy.[7]

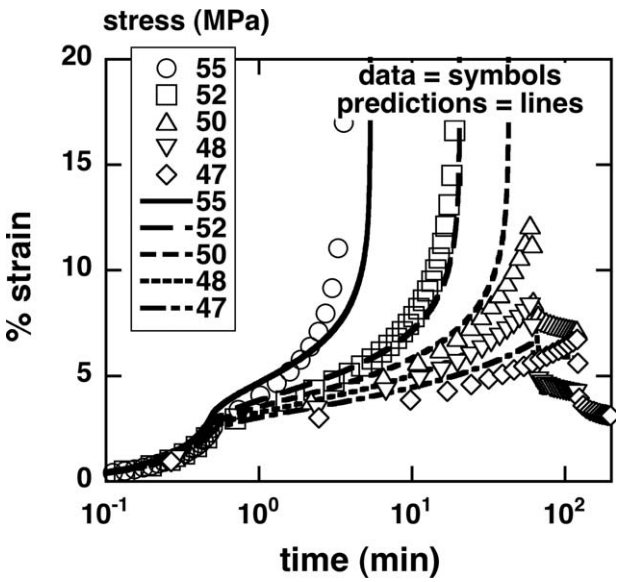

Figure 6 Creep of the DEA-cured epoxy at 23°C.[6]

two relaxation spectra corresponding to the volumetric and shear terms (f_v, f_d), and the usual two WLF coefficients (C_1, C_2). Only two new parameters are required that describe (among other phenomena) the pressure dependence of the glass transition and the acceleration of relaxation rate to applied deformations that produces yield (C_3, C_4).

The model was previously parameterized and accurately predicted a wide range of responses seen in glassy polymers[6–8]: temperature dependent yield in compression and tension, change in the apparent glass transition temperature with pressure, a smooth transition between the glassy and rubbery heat capacities and coefficients of thermal expansion,

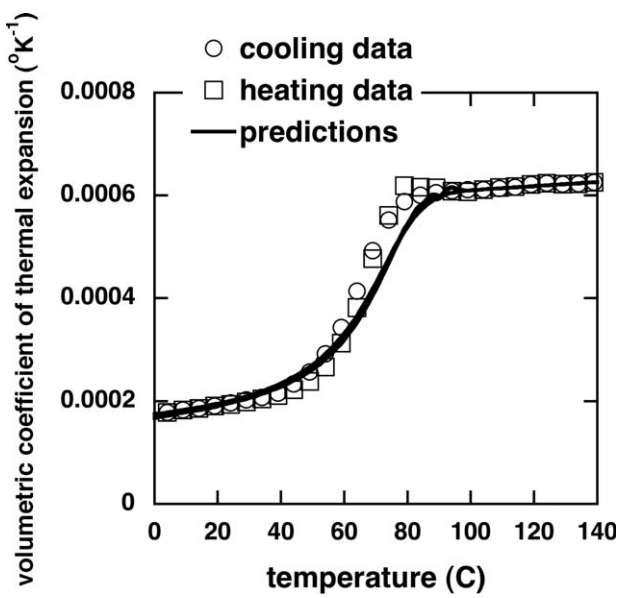

Figure 7 Coefficient of thermal expansion of the DEA-cured epoxy.[7]

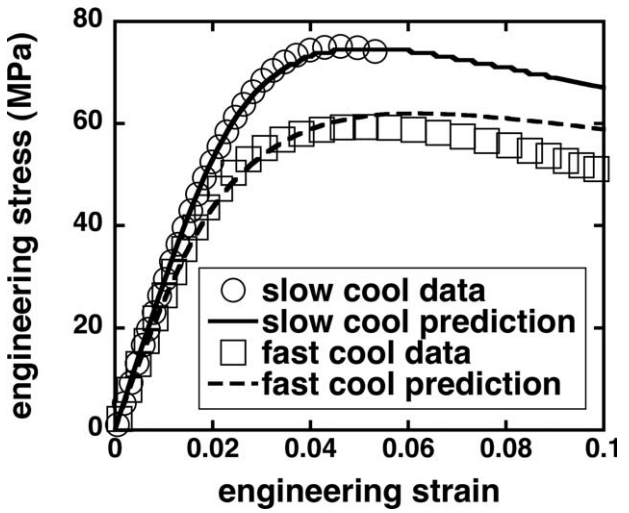

Figure 8 Dependence of the compressive yield stress at 23°C on thermal history.[6]

enthalpy relaxation, increase in the yield stress with time (i.e., physical aging), tensile creep at different temperatures and cooling rates, and even coupled effects such as extreme enthalpy relaxation after application of large stresses. Example predictions are shown in Figures 5–8. In addition, it successfully predicted these responses for several thermosets, a thermoplastic (polycarbonate), and epoxies filled with various particulates past 40 vol %.[9] It has also been extended to predict stresses during thermoset cure by including the extent of reaction as a new dependent variable and tracking the changes in material properties with cure.[10]

This model is unique in its ability to produce consistently accurate predictions for glassy polymers across such a wide range of tests with a unique,

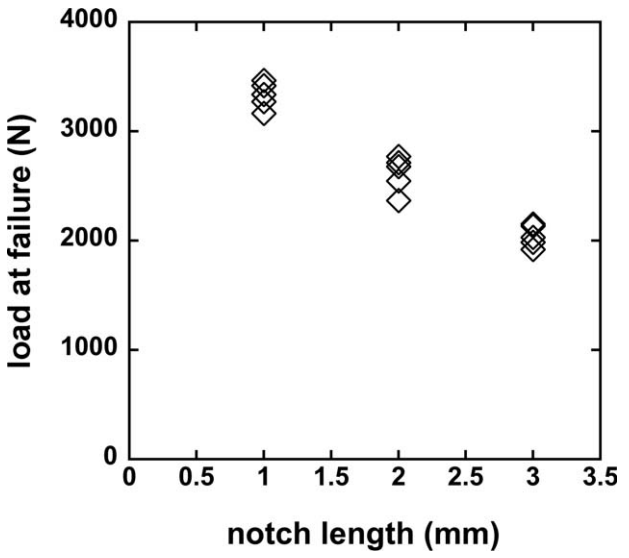

Figure 9 Loads at failure for the double-notched dog bone tests.

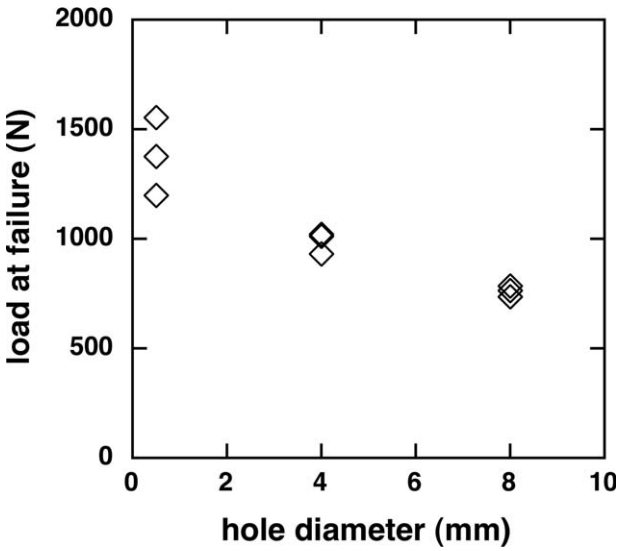

Figure 10 Loads at failure for the cylindrically-notched three-point bend tests.

physically based parameter set. Unlike typical plasticity-based constitutive equations,[11] its viscoelastic foundation adheres to the physics underlying the behavior of glassy polymers by including both shear and volumetric relaxations that depend on environmental conditions through a consistent definition of the potential energy. No irreversible, plastic flow is required to produce yield or creep, thermomechanical response is predicted continuously through the glass transition, and the volumetric relaxations allow important predictions of physical aging, enthalpy relaxation, temperature dependent yield and creep, and a pronounced difference in the magnitudes of compressive and tensile yield stress. In the tests performed here that deformed the samples to failure, gross yield will have occurred near the stress risers, and the tensorial state of stress will be quite complicated and inhomogeneous producing both high

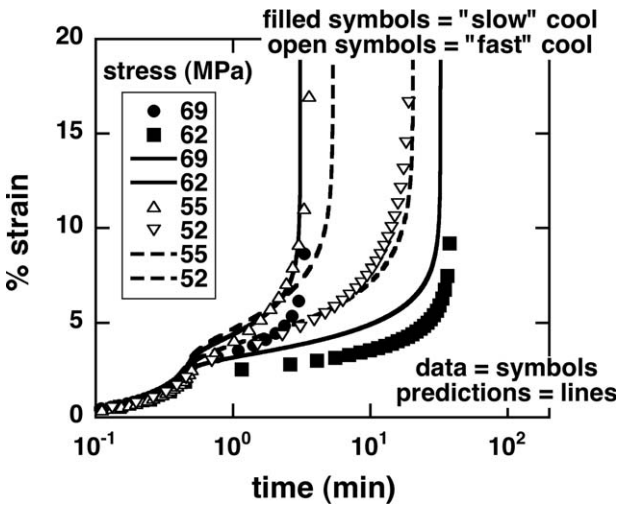

Figure 11 Data and predictions for the creep tests.

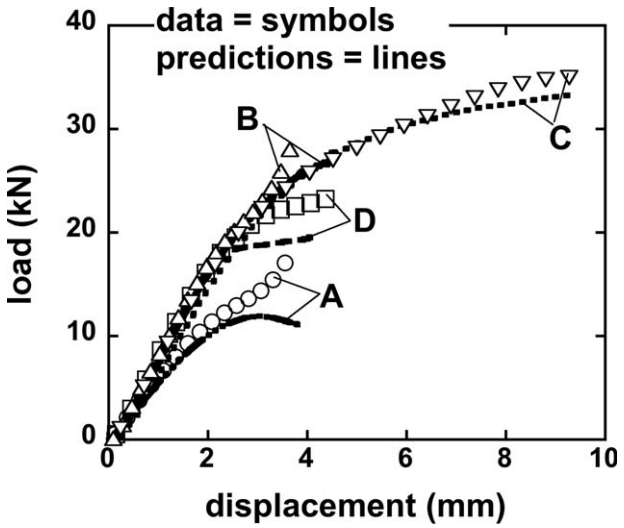

Figure 12 Data and predictions for the ball-into-a-plate tests.

pressures (tensile in the dog bone tests while compressive in the "ball into a plate" tests) and large deviatoric stresses. Models that are created to match one mode of deformation, such as from tensile tests but not necessarily in shear or compression, may not predict stresses accurately at all locations in the failure tests. In addition, models that do not capture temperature and rate dependencies accurately may not predict trends correctly. It is imperative to use an extensively validated, high fidelity constitutive equation to believe the results predicted by the finite element simulations.

The stresses and strains at all elements in each of these simulations at the time of experimental failure were examined to assess if a scalar metric could be

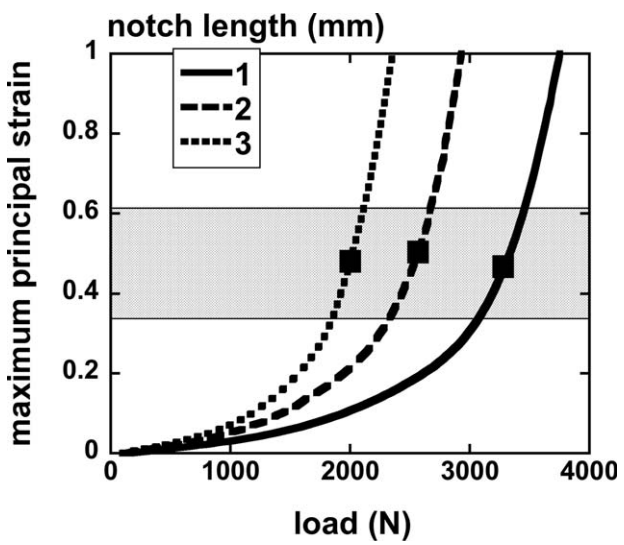

Figure 13 Predicted maximum principal strain versus predicted sample load for the double-notched dog bone samples.

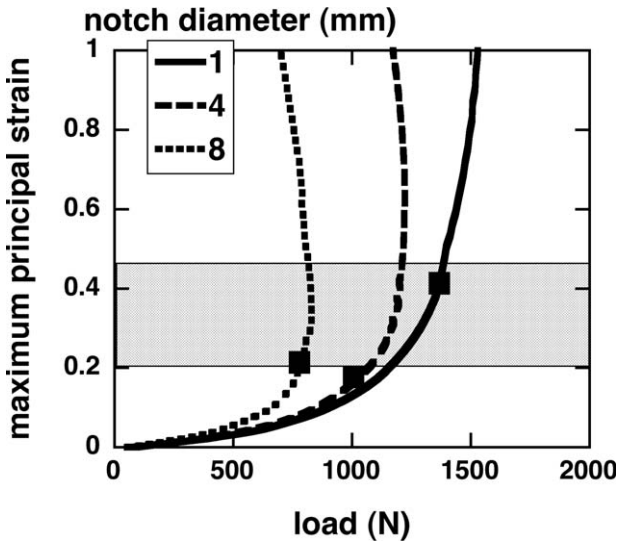

Figure 14 Predicted maximum principal strain versus predicted sample load for the cylindrically-notched 3-point bend samples.

composed that would reach a critical value in each test at the time of observed failure. This metric would then be used as the "failure criterion" in finite element simulations of real components.

Results and implications for samples with geometrical variations tested at room temperature

The measured load-displacement curves for the double-notched dog bone and cylindrically-notched three-point bend tests were linear. The loads at failure for these two families of tests are plotted in Figures 9 and 10. The creep responses are shown in Figure 11, and the load-displacement curves from the ball-into-a- plate tests are shown in Figure 12. Each figure also shows the corresponding nonlinear viscoelastic predictions. For such complicated tests, the predictions match the data well demonstrating the versatility of the constitutive equation (tension, compression, creep, ramp, sensitivity to cooling history).

From these tests, the object now is to construct a scalar metric that will predict failure in all cases. Several types of metrics can be eliminated outright. For example, any stress-based metric will not predict times to fail in creep tests since the stresses are constant by definition. Turning to strain-based metrics, volume strain will not predict failure in both tensile and compressive tests since the sign will change. Perhaps the simplest strain-based criterion would be the maximum principal strain, which is the largest tensile strain in the sample at that time. In Figures 13–15, the predicted maximum principal strain in the element with the largest strain in the sample (i.e,. at the stress riser) is plotted against the predicted sample load for the double-notched dog bone,

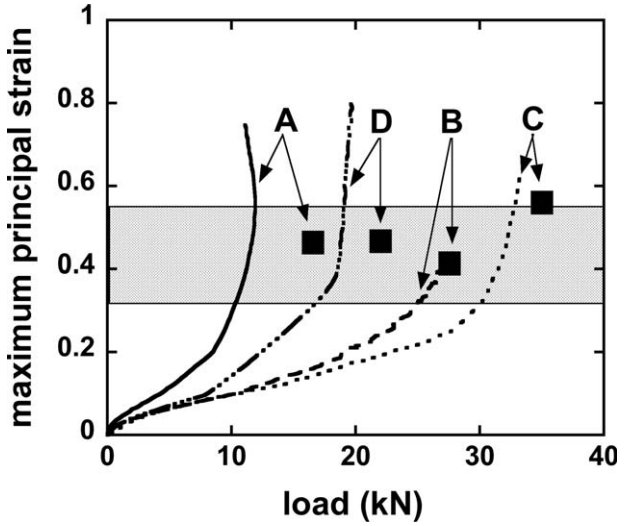

Figure 15 Predicted maximum principal strain versus predicted sample load for the ball-into-a-plate samples A–D.

cylindrically-notched three-point bend, and ball-into-a-plate tests respectively. The experimental load at failure for each test is indicated by a filled square symbol. Shaded regions in each of these plots indicate a range in the maximum principal strain in which the experimental failure loads are captured but the predicted loads vary minimally (roughly ±10%). The creep results are replotted in Figure 16 to show the steepness of the predicted sample strain (also equal to the maximum principal strain) at failure. Therefore, the time at failure in creep is quite insensitive to the exact value of the maximum principal strain postulated at failure, and the shaded region in Figure 16 shows this region of insensitivity.

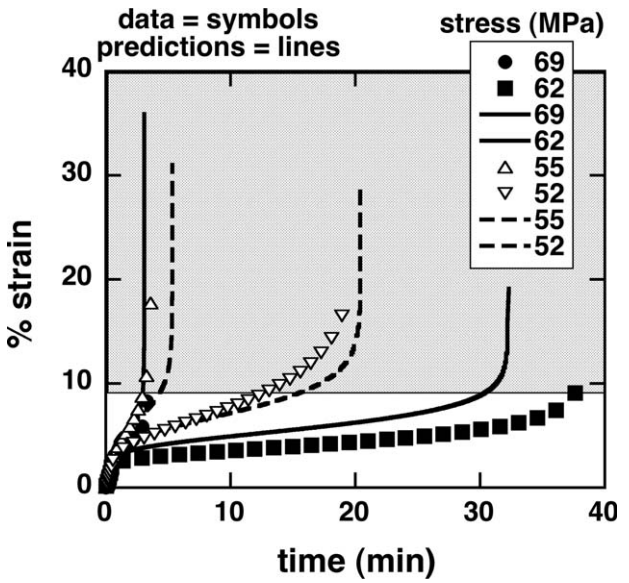

Figure 16 Predicted creep strains versus time.

Reasonable estimates for the minimum and maximum values of the maximum principal strain capturing the observed failure in these tests would be 35 and 45%. The percent errors between the predicted and measured loads or times at failure using these two bounds are plotted in Figure 17. Either bound for the theoretical failure metric gives predictions that agree well with the measured values, and in only two tests does the error exceed 20%. Therefore, the maximum principal strain appears to be an adequate metric of failure in these epoxies for use in finite element analyses over the wide range of test geometries, modes of deformation, and strain histories tested here given, of course, that one uses an accurate constitutive equation to predict the maximum principal strain.

While the goal of this study focused on developing a metric for predicting failure that could be used by analysts to define robust component designs, the results do imply a mechanism underlying the initiation of failure in these epoxies that is most clearly demonstrated in the creep tests (Fig. 16). Creep rates immediately after application of the constant load are relatively slow but increase as time progresses. Failure is coincident with a sharp increase in the creep rates as the sample lengthens catastrophically. This sharp increase is predicted naturally from our nonlinear viscoelastic model in which relaxation rates are dependent on potential energy. Since energy is not directly stress but involves strain as well, the relaxation (i.e., creep) rates increase as strain increases. The dramatic lengthening at failure is a consequence of a nonlinear feedback leading to "run-away" nonlinear viscoelastic creep. This same mechanism should now be apparent in the other sample geometries as seen in Figures 13–15 where the local strains diverge in a similar fashion as the

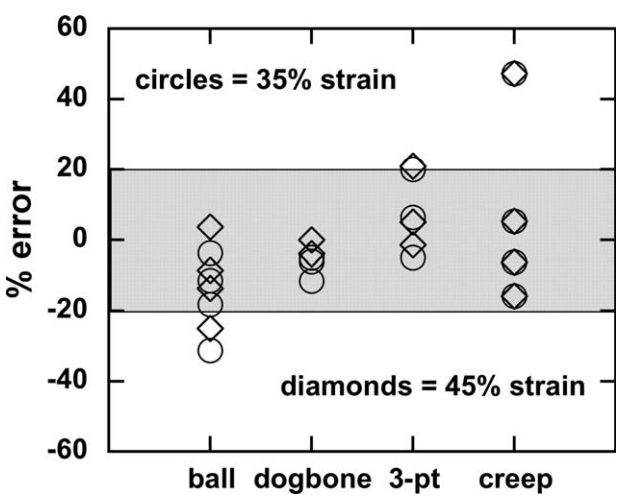

Figure 17 Predicted versus experimental load or times at failure in all tests for bounds on the maximum principal strain failure criterion.

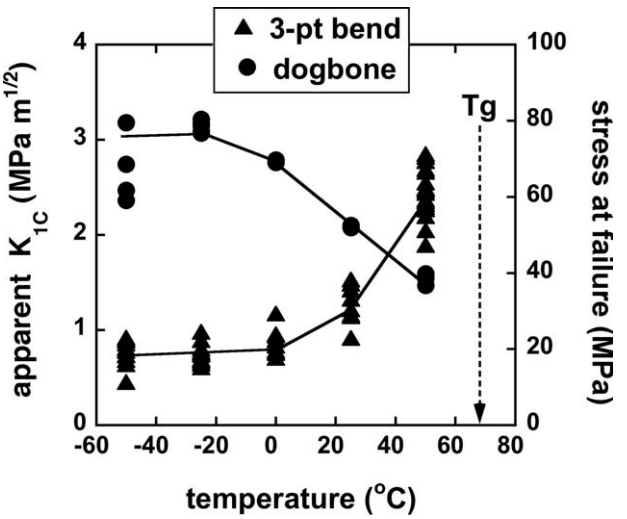

Figure 18 The stress at failure from dog bone tests and the apparent fracture toughness from three-point bend tests have opposite temperature dependencies.

ramped load increases. If this mechanism is responsible for the initiation of cohesive failure, it becomes even more imperative to use a material model that can faithfully capture this run-away viscoelasticity.

For comparison, Gearing and Anand[2] proposed two strain-based failure metrics using an elastic-plastic rather than nonlinear viscoelastic constitutive model for the polymer. "Brittle" fracture was postulated to occur at a critical value of the volumetric strain based on a cavitation mechanism, and "ductile" failure was postulated to occur at a critical value of the effective plastic stretch. A critical plastic stretch of 1.19 was extracted from a dog bone tension test, and a critical volumetric strain of 0.41 was extracted from a notched tension test. Note that a 40% volumetric strain is quite large. These were then applied to two notched four-point bend tests on polycarbonate (a thermoplastic rather than thermoset) at room temperature, and the predicted failures matched the experimental data.

Results and implications for notched three point bend samples tested at different temperatures

While the maximum principal strain failure criterion accurately predicted failure for different geometries and strain histories in tests at room temperature, this criterion also needs to predict failure at different temperatures to be useful in general finite element analyses. Again it is important to distinguish between tests probing the initiation of cohesive failure and those probing crack propagation. Two examples of these different tests would be a dog bone pull test and a precracked, three-point bend test. The stress at failure from dog bone tests and the apparent fracture toughness from three-point bend tests have opposite temperature dependencies as shown in Figure 18 for the DGEBA/DEA epoxy. Whereas fracture mechanics texts detail the precautions required to ensure crack propagation tests give the appropriate toughness values (e.g., thickness requirements) and place limitation on its applicability (e.g., small-scale yielding), no such luxuries are afforded for the prediction of the initiation of cohesive failure. If valid, the maximum principal strain metric must predict failure equally well at different temperatures.

The temperature dependencies of the apparent fracture toughnesses from three-point bend tests with saw cut notches (0.3 mm tip diameter) and with precracks are also seen to be opposite (Fig. 19). So even though the saw cut samples contain a severe stress riser, the fracture mechanics approach cannot be used to predict the apparent toughness, and one wonders if the proposed maximum principal strain criterion can be used.

The experimental loads at failure for the notched three-point bend tests at different temperatures are shown in Figure 20. Loads from the computational simulations of these tests were extracted from elements at the notch tip that first reached maximum strains of either 35 or 45%, which were proposed as bounds on a possible failure metric in the previous section. Both data and predictions show temperature dependences although the predictions change more severely than do the data. Even so, failure predictions using these metrics would be within 20% of the data throughout the temperature range. It is possible that our parameterization of the nonlinear viscoelastic model needs adjustment for these lower temperatures, since it was parameterized with yield data no lower than room temperature. If correct, this

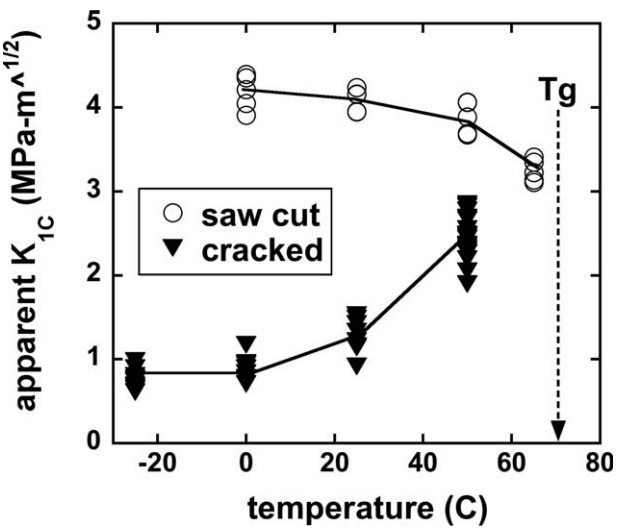

Figure 19 The apparent fracture toughnesses from three-point bend tests with saw cut notches and with precracks have opposite temperature dependencies.

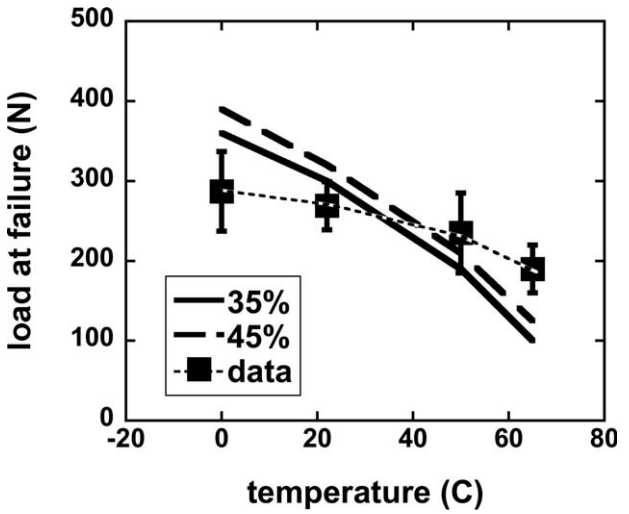

Figure 20 The predicted loads at failure for the saw-cut three-point bend tests show the same trends with temperature as the data.

points out again the need for a quite accurate constitutive model for the polymer.

CONCLUSIONS

A simple metric for predicting the initiation of cohesive failure in an epoxy was determined by examining computational stresses and strains at the point of experimental failure. A physically-based, accurate, nonlinear viscoelastic material model was used to describe the epoxy response, and a wide range of experimental tests were examined including different modes of deformation and temperatures. A critical value of the maximum principal strain of roughly 40% seemed to correlate well with all tests. While this value can apparently be used in finite element simulations of component stresses to guide an engineer toward more robust designs and material selections, it is not necessarily true that this metric implies a physical mechanism for failure. Yet, a mechanism based on "run-away" nonlinear viscoelasticity is consistent with the results. The material constitutive model has been proven to be physically-based, but failure modeling may require higher fidelity computational simulation. For example, the proposed metric cannot predict propagation of an existing crack (more precisely, the temperature dependence of K_{IC}) perhaps due to the complicated nature of a crack tip. While initiation at sharp stress risers that are not actual cracks is easier to model geometrically, the metric developed in this study should be viewed at present as a useful quantity for design engineers.

The authors would like to acknowledge the assistance provided by New Mexico Tech undergraduate students, Annie Hohmann, Timothy Schutt, and Isabel McCoy, who prepared samples and ran tests providing data for determining the temperature dependence of the three point bend and dog bone geometries. Sandia is a multiprogram laboratory operated by Sandia Corporation, a Lockheed Martin Company, for the United States Department of Energy's National Nuclear Security Administration under contract DE-AC04-94AL85000.

References

1. Nemeth, N. N.; Powers, L. M.; Janosik, L. A.; Gyekenyes, J. P. In Advanced Ceramic Matrix Composites: Design Approaches, Testing and Life Prediction Methods, Generazio, E. R., Ed.; CRC Press: London, 1996, Chapter 1.
2. Gearing, B. P.; Anand, L. Int J Solids Struct 2004, 41, 827.
3. Adolf, D. B.; Martin, J. E.; Chambers, R. S.; Burchett, S. N.; Guess, T. R. J Mat Res 1998, 13, 530.
4. Caruthers, J. M.; Adolf, D. B.; Chambers, R. S.; Shrikhande, P. Polymer 2004, 45, 4577.
5. Budzien, J.; McCoy, J. D.; Adolf, D. B. J Chem Phys 2004, 121, 10291.
6. Adolf, D. B.; Chambers, R. S.; Neidigk, M. A. Polymer 2009, 45, 4599.
7. Adolf, D. B.; Chambers, R. S.; Caruthers, J. M. Polymer 2004, 45, 4599.
8. Adolf, D. B.; Chambers, R. S.; Flemming, J. J Rheol 2007, 51, 517.
9. Adolf, D. B.; Chambers, R. S. J Polym Sci B 2005, 43, 3135.
10. Adolf, D. B.; Chambers, R. S. J Rheol 2007, 51, 23.
11. Hill, R. The Mathematical Theory of Plasticity (Oxford Classic Series); Oxford University Press: Oxford, 1998.